Journal of the Korean Ceramic Society
Vol. 53, No. 5, pp. 489~493, 2016.

http://dx.doi.org/10.4191/kcers.2016.53.5.489

# Symmetrical Solid Oxide Electrolyzer Cells (SOECs) with $La_{0.6}Sr_{0.4}Co_{0.2}Fe_{0.8}O_3$ (LSCF)-Gadolinium Doped Ceria (GDC) Composite Electrodes

**Kyoung-Jin Lee*, Min-Jin Lee*, Seok-hoon Park**, and Hae-Jin Hwang*,†**

**Department of Materials Science and Engineering, Inha University, Incheon 22212, Korea*

***Department of Environmental Engineering, Anyang University, Anyang 14028, Korea*

(Received August 10, 2016; Revised September 20, 2016; Accepted September 21, 2016)

**ABSTRACT**

Scandia ($Sc_2O_3$)-stabilized zirconia (ScSZ) electrolyte-supported symmetrical solid oxide electrolyzer cells (SOECs), in which lanthanum strontium cobalt ferrite (LSCF)-gadolinia ($Gd_2O_3$)-doped ceria (GDC) composite materials are used as both the cathode and anode, were fabricated and their high temperature steam electrolysis (HTSE) performance was investigated. Current density-voltage curves were obtained for cells operated in 10% $H_2O$/90% Ar at 750, 800, and 850ºC. It was possible to determine the ohmic, cathodic, and anodic contributions to the total overpotential using the three-electrode technique. The HTSE performance was significantly improved in the symmetrical cell with LSCF-GDC electrodes compared to the cell consisting of an Ni-YSZ cathode and LSCF-GDC anode. It was found that the overpotential due to the LSCF-GDC cathode largely decreased and, at a given current density, the total cell voltage decreased, which resulted in the enhanced hydrogen production rate in the symmetrical cell.

***Key words : HTSE, SOECs, Symmetrical cell, LSCF-GDC, Hydrogen production rate***

## 1. Introduction

High temperature steam electrolysis (HTSE) using a solid oxide electrolyzer cell (SOEC) is known to be a more efficient way to produce hydrogen than conventional water electrolysis because the electricity consumption can be significantly reduced when the electrolyzer cell is operated at high temperature.[1,2] Another advantage of SOECs is that they can operate reversibly as solid oxide fuel cells (SOFC), producing electricity with high efficiency by consuming stored hydrogen.[3]

Many research works have been carried out for the development of an energy efficient high temperature solid oxide fuel cell (SOFC), in which cells employ a reverse operation of SOEC. Various materials, processing techniques, and cell or stack designs have been proposed and optimized over the past few decades.[4-6] Although the technologies developed for SOFC have also been found to be useful for the development of SOEC, more sophisticated material design and performance characterization of SOEC is needed for more cost-effective electrolytic hydrogen production.[7,8]

Nickel and yttria-stabilized zirconia (Ni–YSZ) cermet has been utilized as the most common cathode material of SOEC due to its high catalytic activity, sufficient conductivity, and mechanical/chemical compatibility with other components. However, the Ni-YSZ cermet requires a large amount of hydrogen to avoid oxidation to nickel oxide (NiO) in the presence of water vapor at high temperatures. Some researchers have reported on the electrode performance of perovskite-type oxides such as lanthanum-doped strontium titanate (LST) and lanthanum strontium manganese chromite (LSMC).[9,10] They addressed the idea that the oxide cathode exhibited enhanced performance compared to the Ni-YSZ cermet.

In this study, an electrolyte-supported SOEC consisting of an $Sc_2O_3$-stabilized $ZrO_2$ (ScSZ) electrolyte and $La_{0.6}Sr_{0.4}Co_{0.2}Fe_{0.8}O_{3-d}$ (LSCF)-$Gd_2O_3$-doped $CeO_2$ (GDC) electrodes was fabricated and its hydrogen production performance was investigated. Also, we tried to evaluate the polarization losses with respect to water vapor reduction and oxygen ion oxidation over the LSCF-GDC composite electrode.

## 2. Experimental Procedure

Two types of electrolyte supported electrolyzer cells, LSCF-GDC/GDC/ScSZ/GDC/LSCF-GDC (cell A, hereafter) and Ni-YSZ/ScSZ/GDC/LSCF-GDC (cell B, hereafter), were fabricated in this study. The cell configuration used in this study is shown schematically in Fig. 1. Commercially available ScSZ (88 mole% $ZrO_2$-8 mole% $Sc_2O_3$-2 mole% $Y_2O_3$, Kceracell, Korea), LSCF-GDC (Fuel Cell Materials, USA), GDC (Anan Kasei Co. Ltd., Japan), and Ni-YSZ (Fuel Cell Materials, USA) powders were used for the cell preparation.

First, the ScSZ powder was uniaxially pressed into a pellet and sintered at 1500°C for 5 h in air. An ScSZ disk with

†Corresponding author : Hae-Jin Hwang
E-mail : hjhwang@inha.ac.kr
Tel : +82-32-860-7521 Fax : +82-32-862-4482

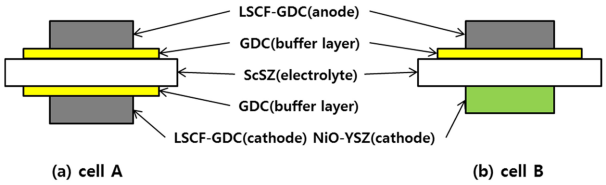


**Fig. 1.** Schematic picture showing the cell configuration used in this study.

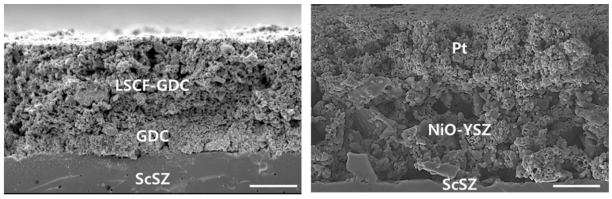


**Fig. 2.** Cross-sectional SEM images for the cathode interfaces of cell A (a) and cell B (b) (scale bar: 10 μm).

a diameter of 22 mm and a thickness of 0.2 mm was obtained. LSCF-GDC and GDC pastes were prepared by mixing the powders and an organic vehicle (a-terpinol, *n*-butyl acetate, and ethyl cellulose). The weight ratio of each powder to the organic vehicle was 60:40. The GDC buffer layer was formed using the GDC paste on the ScSZ disk via a screen printing technique followed by heat-treatment at 1200°C for 2 h in air. The LSCF-GDC layers were also screen-printed on the GDC buffer layer and were heat-treated at 1000°C for 2 h in air. The area of the electrode was 1 $cm^2$. A current-collecting Pt layer containing 15 wt% YSZ was further formed on the LSCF-GDC electrodes via a screen printing method. Pt wire was used to make the reference electrode on the side of the ScSZ electrolyte disk.

The alumina tubes on both the top and bottom sides of the electrolyzer cell were sealed with Pyrex glass rings. The cell was then placed inside a furnace and heated at 850°C to allow for the sealing glass to be softened. 10% steam/Ar and 10% steam/$H_2$ were supplied to the LSCF-GDC and Ni-YSZ cathodes, respectively. The water vapor partial pressure of the cathode gas mixture was determined by the temperature of the water bath inside the humidifier. On the other hand, the anode was supplied with air. The flow rates of 10% steam/Ar, 10% steam/$H_2$, and air were 100 ml $min^{-1}$.

The current density-voltage curves were measured with a three probe method using electrochemical testing equipment (IM6e, Zahner, Germany). The three Pt wires from the anode, cathode, and reference electrodes were connected to the working, counter, and reference terminals of the testing equipment, respectively. Hydrogen production rate of the SOEC was calculated using Faraday's law, assuming 100% current efficiency. The microstructure was monitored by field-emission scanning electron microscopy (FE-SEM, S-4300, Hitachi).

## 3. Results and Discussion

Figure 2 shows cross-sectional SEM images for the cathode-electrolyte interface of cell A (a) and cell B (b). The LSCF-GDC layers exhibited a porous microstructure, while the GDC buffer layer were sufficiently densified and adhered well to the ScSZ electrolyte. The thicknesses of the LSCF-GDC, Ni-YSZ, and GDC layers were estimated to be approximately 18, 25, and 10 μm, respectively. As can be seen in Fig. 2(a), the LSCF-GDC cathode had a homogeneous particle size distribution; the particle size of the

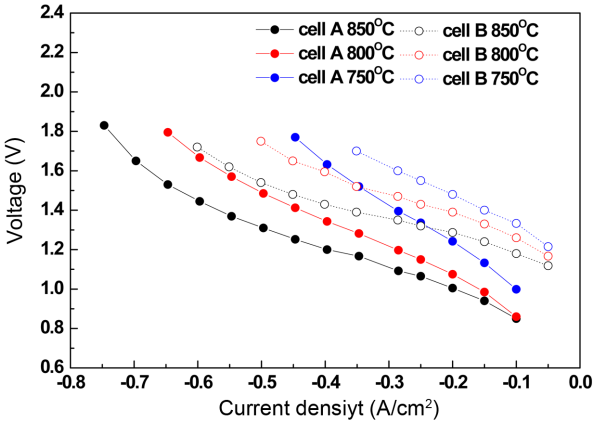


**Fig. 3.** Current density-voltage curves of cells A and B at 750, 800, and 850°C.

LSCG-GDC cathode was approximately 0.5 to 1 mm.

On the other hand, the morphology of the NiO particles was found to be slightly irregular and their size was much larger than that of the LSCF-GDC cathode. This observed phenomenon might be associated with the heat-treatment temperature difference. The LSCF-GDC and NiO-YSZ layers were coated on the ScSZ electrolyte disk and subsequently heat-treated at 1000 and 1400°C, respectively. In the case of the NiO-YSZ cathode, the heat-treatment at high temperature resulted in particle growth and agglomeration.

Current density-voltage curves of two electrolyzer cells (cell A and cell B) operated under SOEC mode at 750, 800, and 850°C are shown in Fig. 3. As is evident in Fig. 3, asymmetry in the current density-voltage curves appeared. In the SOFC mode, the voltage decreased almost linearly with increasing of the current density, while the current density-voltage characteristics in the SOEC mode seem to be more complicated than those in the SOFC mode. The slope of the current density-voltage curve is steep in the low current density range; it then becomes modest between -0.2 and -0.4 A/$cm^2$, and again increases steeply with increasing of the current density. In addition, the low voltage at a given current density, i.e., the significantly superior steam electrolysis performance of cell A based on the LSCF-GDC cathode compared to cell B based on the Ni-YSZ cathode suggests that the LSCF cathode exhibits better catalytic activity for the reduction of steam into hydrogen.

The cell voltage shown in Fig. 3 was recorded by measuring the voltage between two electrodes; it can be written by

starting with the thermodynamically predicted voltage of the cell and then subtracting the voltage losses, such as the ohmic, activation, and concentration losses. The voltage loss due to the ohmic resistance of the cell can be estimated by multiplying the ohmic resistance, which can be determined from the impedance spectrum of the cell, by the current density. In addition, the activation loss of each electrode can be obtained by measuring the voltage between the anode and the reference and between the cathode and the reference.

The resulting ohmic loss, cathodic voltage (LSCF-GDC for cell A and Ni-YSZ for cell B), and anodic voltage (LSCF-GDC for both cells) are shown in Fig. 4(a), (b), and (c). The ohmic loss, originating mainly from the resistance of the ScSZ electrolyte, was significant in both cells A and B. The slightly high ohmic loss in cell A compared to that in cell B can be ascribed to the low electrical conductivity of the LSCF-GDC cathode and the presence of the GDC buffer layer in the cathode. Since the electrical conductivity of the GDC layer is relatively high at the cell operating temperatures and because its thickness is very thin, the contribution of the GDC buffer layer to the total cell resistance must be small, though some pores in the GDC layer can affect the resistance of cell A.

On the other hand, the cathodic voltage is much lower in cell A than in cell B, which indicates that the LSCF-GDC may be promising for use as an SOEC cathode. An interesting feature that can be observed in Fig. 4(b) is that the cathodic voltage of cell A increased very modestly as the current density increased from -0.1 to -0.6 A/cm$^2$. This result means that the activation barrier for the reduction of steam into hydrogen is enormously reduced in the LSCF-GDC cathode of cell A.

The enhanced cell performance observed in Fig. 4 can be explained by two factors; one is the microstructural features in cell A and the other is the increased catalytic activity for the reduction of steam over the LSCF-GDC cathode. As was mentioned in the earlier section (Fig. 2), the LSCF-GDC cathode has a finer and more homogenous microstructure than that of the NiO-YSZ cathode. This microstructure can allow a prolonged triple phase boundary length and a resulting reduced polarization resistance at the cathode. In addition, LSCF-GDC showed a higher oxygen vacancy concentration compared to NiO-YSZ, most likely yielding increased oxide ion mobility and availability of adsorption sites in LSCF-GDC.[11] This can be another reason for the decreased cathodic voltage observed in Fig. 4(b).

As was described in the previous section, the ohmic loss and the electrode overpotentials of two cells were determined for each current density. The total sum of the overpotentials was calculated and plotted in Fig. 5. As can be seen in Fig. 5, the cell voltage measured between the two electrodes agrees well with the total sum of the overpotentials.

In the case of cell B, a cell voltage of 1.4 V corresponds to a current density of -0.35 A/cm$^2$. Under these operating conditions, the ohmic, cathodic (Ni-YSZ), and anodic (LSCF-GDC) overpotentials were 158 mV (45%), 156 mV (44%), and 37mV (11%), respectively. It is clear that the overpotential resulting from the Ni-YSZ cathode contributes to the

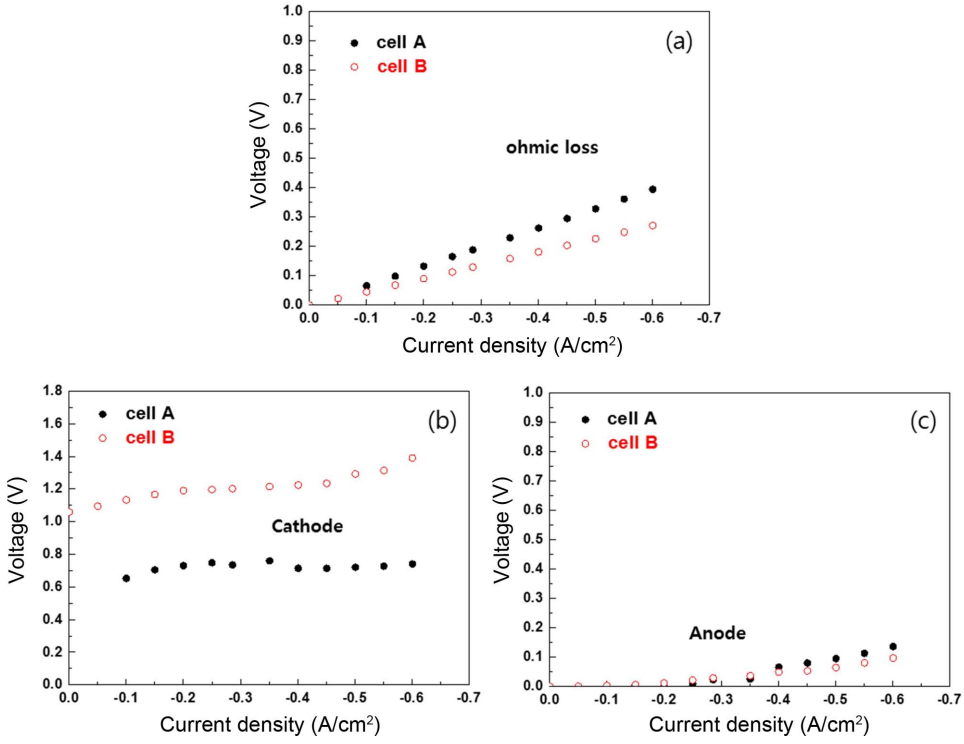


**Fig. 4.** Current density-voltage curves of cells A and cell B measured at 850°C; (a) ohmic loss, (b) cathodic voltage, (c) anodic voltage.

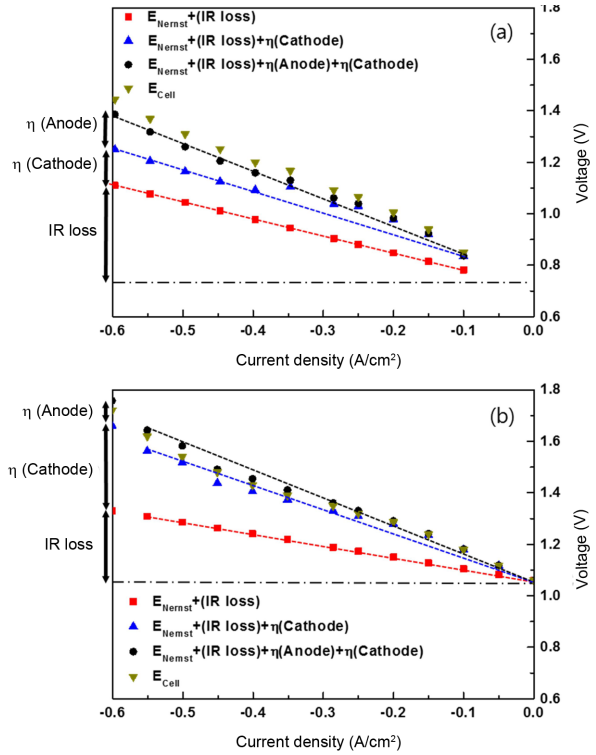


**Fig. 5.** Current density-voltage curve of cell A (a) and cell B (b) measured at 850°C, and curve split into ohmic loss (IR loss) and electrode overpotentials.

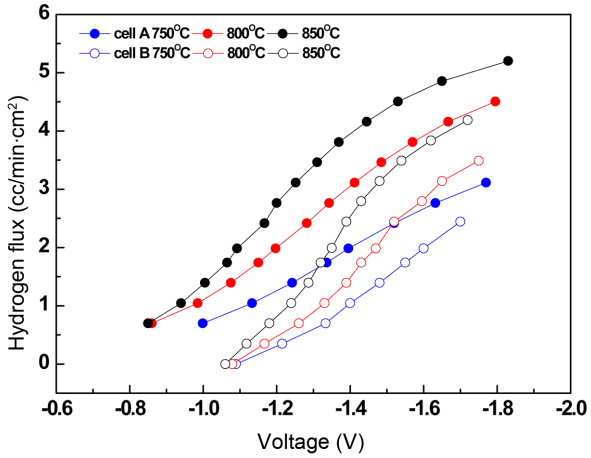


**Fig. 6.** Hydrogen production rate vs. voltage curves at 750, 800, and 850°C.

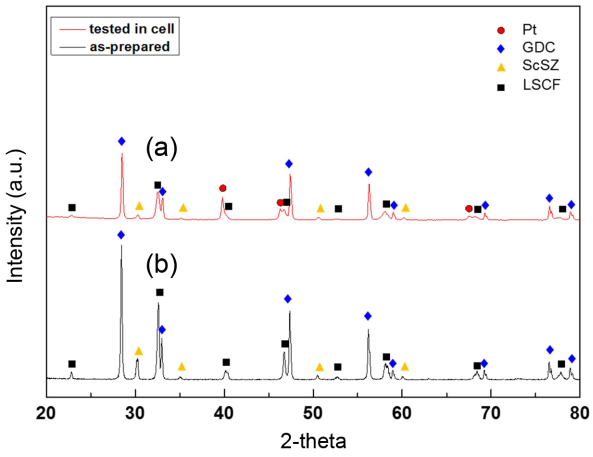


**Fig. 7.** XRD patterns of LSCF-GDC cathode: (a) as-prepared LSCF-GDC, (b) LSCF-GDC after cell performance measurement.

main part of the total voltage loss. Considering that the cell used in this study is an electrolyte (0.2 mm in thickness)-supported cell, 39% of the ohmic contribution seems to be reasonable. However, the large Ni-YSZ overpotential may be problematic. The cause of the large overpotential might be the low vapor pressure of water (10%) and the absence of a functional layer, which layers are usually used for normal SOFC or SOEC cells. In addition, the Ni-YSZ overpotential contributes to a much larger extent at high current densities, suggesting the presence of concentration loss at high current densities.

On the other hand, the cathodic polarization resistance decreased in cell A, while the ohmic and anodic polarization resistances slightly increased. As was mentioned in previous sections, this result is ascribed to the low electrical conductivity of the LSCF-GDC cathode and the low density of the GDC buffer layer in cell A.

Figure 6 shows the hydrogen production rates of cell A and cell B at 750, 800, and 850°C. The hydrogen production rate increases as the applied voltage increases and also as the operating temperature increases. At a given voltage, the hydrogen production rate was found to have a two-fold higher value in cell A than in cell B. For example, the hydrogen production rates of cell A and cell B were 3.5 and 1.5 sccm/cm$^2$, respectively, with an applied voltage of 1.3 V at 850°C and 10% $H_2O$.

It has been reported that LSCF can be used as an anode material of SOFCs operated in hydrogen at 500°C[12,13] or with hydrocarbon fuels in the intermediate temperature range of 550 ~ 700°C.[14,15] Those studies addressed the idea that LSCF or LSCF-GDC displayed good phase stability, depending on the operating temperature or atmosphere. In order to confirm the stability of the LSCF-GDC in the cathodic atmosphere of the SOEC mode, phase analysis was carried out for the LSCF-GDC sample after the cell performance measurement. XRD patterns of the as-prepared LSCF-GDC and LSCF-GDC cathode tested in cell A are shown in Fig. 7. It was found that the as-prepared LSCF-GDC consists of LSCF and GDC phases; there were no unwanted or reaction phases. In comparison, as can be seen in Fig. 7(b) and Fig. 7(a), there was no significant change after the cell operation in 10% $H_2O$/90% Ar at 850°C. This observed result suggests that the LSCF-GDC is stable in the operation conditions of the SOEC, although a long-term stability test should be carried out in the future. It is considered that water vapor in the cathode can increase the oxygen partial pressure of the cathode, leading to the enhanced

phase stability of the LSCF in hydrogen atmosphere.

## 4. Conclusions

Symmetrical solid oxide electrolyzer cells (SOECs) consisting of an ScSZ electrolyte and LSCF-GDC electrodes were fabricated. Their HTSE performances were evaluated at 750, 800, and 850ºC and compared with that of the Ni-YSZ/ScSZ/LSCF-GDC cells. The total cell voltage was significantly reduced in the symmetrical cell with LSCF-GDC electrodes (cell A) operated in 10% $H_2O$/90% Ar, compared to cell B operated in 10% $H_2O$/90% $H_2$. This observed result suggests that the LSCF-GDC can be used as a cathode material of SOECs. The phase stability of the LSCF-GDC in the cathode atmosphere, such as 10% $H_2O$/90% Ar, was confirmed by XRD analysis. The hydrogen flux of the symmetrical cell operated at 850ºC was 3.5 cc/min·$cm^2$ at -1.3 V, which is about 2.5 times higher than that of the cell with the Ni-YSZ cathode. In order to enhance the performance of the symmetrical cell, it is necessary to reduce the electrolyte thickness, i.e., that of the electrode-supported cell, and ensure microstructure control of the LSCF-GDC cathode.

## Acknowledgments

This work was supported by the Fundamental R&D Program for Core Technology of Materials (No.10051006) of the Korea Evaluation Institute of Industrial Technology (KEIT), Republic of Korea.

This work was supported by a National Research Foundation of Korea (NRF) grant funded by the Korean Government (MEST) (No. 2010-0029861).

## REFERENCES

1. M. Ni, M. K. H. Leung, and D. Y. C. Leung, "Technological Development of Hydrogen Production by Solid Oxide Electrolyzer Cell (SOEC)," *Int. J. Hydrogen Energy*, **33** [9] 2337-54 (2008).
2. W. Donitz, E. Edle, R. Streicher, H. Wendt, "Electrochemical Hydrogen Technologies: Electrochemical Production and Combustion of Hydrogen," pp. 213 in Electrochemical Hydrogen Technologies, Elsevier, Amsterdam, Netherland, 1990.
3. M. A. Laguna-Bercero, S. J. Skinner, and J. A. Kilner, "Performance of Solid Oxide Electrolysis Cells Based on Scandia Stabilised Zirconia," *J. Power Sources,* **192** [1] 126-31 (2009).
4. J. Kong, Y. Zhang, C. Deng, and J. Xu, "Synthesis and Electrochemical Properties of LSM and LSF Perovskites as Anode Materials for High Temperature Steam Electrolysis," *J. Power Sources*, **186** [2] 485-89 (2009).
5. N. Q. Minh, "Development of Reversible Solid Oxide Fuel Cells (RSOFCs) and Stacks Electrolysis and Other Applications," *ECS Trans.,* **35** [1] 2897-904 (2011).
6. D. Grondin, N. Grunbaum, J. Deseure, and P. Ozil, "The Use of Conventional SOFC Electrodes in High Temperature Water Electrolysis Mode: An Electrochemical Study of Ni-Cermet and LSM Cell Designs, Processing and Performance," *ECS Trans.*, **25** [2] 1007-14 (2009).
7. A. Brisse, J. Schefold, and M. Zahid, "High Temperature Water Electrolysis in Solid Oxide Cells," *Int. J. Hydrogen Energy*, **33** [20] 5375-82 (2008).
8. Y. Bo, Z. Wenqiang, X. Jingming, and C. Jing, "Status and Research of Highly Efficient Hydrogen Production through High Temperature Steam Electrolysis at INET," *Int. J. Hydrogen Energy*, **35** [7] 2829-35 (2010).
9. O. A. Marina, L. R. Pederson, M. C. Williams, G. W. Coffey, K. D. Meinhardt, C. D. Nguyen, and E. C. Thomsena, "Electrode Performance in Reversible Solid Oxide Fuel Cells," *J. Electrochem. Soc.,* **154** [5] B452-59 (2007).
10. X. Yang and J. T. S. Irvine, "$(La_{0.7}5Sr_{0.25})_{0.95}Mn_{0.5}Cr_{0.5}O_3$ as the Cathode of Solid Oxide Electrolysis Cells for High Temperature Hydrogen Production from Steam," *J. Mater. Chem.,* **18** [20] 2349–54 (2008).
11. G. Tsekouras, D. Neagu, and J. T. S. Irvine, "Step-Change in High Temperature Steam Electrolysis Performance of Perovskite Oxide Cathodes with Exsolution of B-site Dopants," *Energy Environ. Sci.,* **6** [1] 256-66 (2013).
12. B. K. Lai, K. Kerman, and S. Ramanathan, "Nanostructured $La_{0.6}Sr_{0.4}Co_{0.8}Fe_{0.2}O_3$/$Y_{0.08}Zr_{0.92}O_{1.96}$/$La_{0.6}Sr_{0.4}Co_{0.8}Fe_{0.2}O_3$ (LSCF/YSZ/LSCF) Symmetric Thin Film Solid Oxide Fuel Cells," *J. Power Sources*, **196** [4] 1826-32 (2011).
13. T. J. Huang and C. M. Chen, "Syngas Reactivity over $(LaAg)(CoFe)O_3$ and Ag-added $(LaSr)(CoFe)O_3$ Anodes of Solid Oxide Fuel Cells," *J. Power Sources,* **196** [5] 2545-50 (2011).
14. A. Hartley, M. Sahibzada, M. Weston, I. S. Metcalfe, and D. Mantzavinos, "$La_{0.6}Sr_{0.4}Co_{0.2}Fe_{0.8}O_3$ as the Anode and Cathode for Intermediate Temperature Solid Oxide Fuel Cells," *Catalysis Today,* **55** [1] 197-204 (2000).
15. A. Sin, E. Kopnin, Y. Dubitsky, A. Zaopo, A. S. Arico, L. R. Gullo, D. La Rosa, and V. Antonucci, "Stabilisation of Composite LSFCO–CGO Based Anodes for Methane Oxidation in Solid Oxide Fuel Cells," *J. Power Sources*, **145** [1] 68-73 (2005).